Genetic variation for ontogenetic shifts in metabolism underlies physiological homeostasis in *Drosophila*

Omera B. Matoo*, Cole R. Julick, and Kristi L. Montooth

School of Biological Sciences, University of Nebraska-Lincoln, NE 68502

* Corresponding author:

Omera B. Matoo

1104 T Street

Lincoln, NE 68588-0118

omatoo2@unl.edu

Abstract

Organismal physiology emerges from metabolic pathways and structures that can vary across development and among individuals. Here we tested whether genetic variation at one level of physiology can be buffered at higher levels during development by the inherent capacity for homeostasis in physiological systems. We found that the fundamental scaling relationship between mass and metabolic rate, as well as the oxidative capacity per mitochondria, differed significantly across development in the fruit fly *Drosophila*. However, mitochondrial respiration rate was maintained across development at similar levels. Furthermore, genotypes clustered into two types—those that switched to aerobic, mitochondrial ATP production before the second instar and those that relied on anaerobic production of ATP via glycolysis through the second instar. Despite genetic variation for the timing of this metabolic shift, second-instar metabolic rate was more robust to genetic variation than was the metabolic rate of other instars. We also found that a mitochondrial-nuclear genotype with disrupted mitochondrial function both increased aerobic capacity more through development and relied more heavily on anaerobic ATP production relative to wildtype genotypes. By taking advantage of both ways of making ATP, this genotype maintained mitochondrial respiratory capacity, but also generated more free radicals and had decreased mitochondrial membrane potential, potentially as a physiological-defense mechanism. Taken together, the data revealed that genetic defects in core physiology can be buffered at the organismal level via physiological compensation and that natural populations likely harbor genetic variation for distinct metabolic strategies in development that generate similar organismal outcomes.

Keywords: mtDNA, metabolism, oxidative phosphorylation, reactive oxygen species

Introduction

Metabolism is the sum total of biochemical processes by which organisms use energy to sustain life and fuel reproduction, and an individual's metabolic rate is often interpreted as an integrated measure of its "pace of life"(Glazier, 2005, 2014, 2015). Early surveys of molecular variation revealed a surprising amount of genetic variation segregating in natural populations at the loci encoding these biochemical processes (Harris, 1966; Hubby and Lewontin, 1966; Lewontin and Hubby, 1966), a pattern that has been historically used to advocate both for the predominance of classical mutation, drift and purifying selection forces (Kimura 1983) and for the maintenance of variation through selection (Gillespie, 1999) (reviewed by Charlesworth and Charlesworth, 2016). Subsequent surveys revealed substantial quantitative genetic variation in metabolic enzyme activities within species, arising from both molecular variation at enzyme-encoding loci, as well as trans-acting and epistatic variation throughout the genome (Clark and Wang, 1997; Clark *et al.*, 1995a, 1995b; Laurie-Ahlberg *et al.*, 1980, 1982; Mitchell-Olds and Pedersen, 1998; Montooth *et al.*, 2003). In a few cases, this biochemical variation has been linked to variation at higher levels of physiological or organismal performance (Crawford and Oleksiak, 2007; Laurie-Ahlberg *et al.*, 1982; Montooth *et al.*, 2003; Watt *et al.*, 1983) and in some cases may be adaptive (Tishkoff *et al.*, 2001; Verrelli and Eanes, 2001; Watt, 1977; Watt *et al.*, 2003). However, we still lack a general mechanistic understanding of how genetic variation in the pathways of metabolism is transformed up the hierarchical levels of biological organization to result in variation for the organismal performance traits that determine fitness. This understanding is important for consideration of metabolism as an adaptive phenotype and for predicting how selection on metabolic performance will shape variation in genomes.

A challenge to connecting genetic variation in biochemical processes to metabolic performance, is that metabolism is an emergent property of interacting biochemical, structural, regulatory and physiological systems, often arranged in hierarchical functional modules (Barabási and Oltvai, 2004; Jeong *et al.*, 2000; Ravasz *et al.*, 2002; Strogatz, 2001). In addition, metabolic enzymes and metabolites have potential "moonlighting" functions in the signaling that underlies metabolic homeostasis (Marden, 2013; Boukouris *et al.*, 2016). The capacity for homeostasis in physiological systems, also suggests that genetic variation in biochemical processes at one level of the energetic hierarchy may not necessarily result in organismal fitness variation. In other words, the physiological regulatory processes that maintain energy homeostasis may provide stability in metabolic trajectories, in an analogous way to the canalized developmental trajectories envisioned by Waddington (Meiklejohn and Hartl, 2002; Waddington, 1942, 1957). Furthermore, a diversity of biochemical pathways may be available to achieve similar energetic outputs. Finally, the hierarchical biological processes that contribute to metabolism are influenced by both extrinsic (e.g., temperature, resource availability, habitat, and infection status) and intrinsic (e.g., genotype, life stage, sex, activity level, and reproductive status) factors [reviewed (Glazier, 2005)], such that genetic variation in biochemical processes may affect organismal performance and fitness in only a subset of conditions. Such conditionally neutral variation is expected to experience less effective selection, as it will be seen by selection in only a fraction of contexts (Van Dyken and Wade, 2010).

Development is a potentially important context for the expression of genetic variation in metabolism. During development, organisms partition energetic resources between the competing demands of growth, development, maintenance, and storage for future reproduction. Energy homeostasis during development is largely achieved by feedback controls where energy-

demand processes increase the concentration of ADP, which can then be fed as a substrate for energy-supply processes to generate ATP. As key metabolic organelles, the mitochondria play a central role in the energy supply-demand balance. Not only the abundance and activity of mitochondria, but also the surface area, membrane composition , and cellular network structure of mitochondria have been reported to affect metabolism (Miettinen and Björklund, 2017; Porter and Brand, 1993; Porter *et al.*, 1996). In addition, both mitochondrial and nuclear genomes interact closely to form the protein complexes of oxidative phosphorylation (OXPHOS) that drive aerobic ATP production, creating the potential for inter-genomic epistasis to underlie variation in metabolic phenotypes. At present, our understanding of the how the underlying genetic architecture and its variation affects metabolism is incomplete; but studies indicate that both nuclear DNA (nDNA) (Montooth et al., 2003; Nespolo *et al.*, 2007; Tieleman *et al.*, 2009), mitochondrial DNA (mtDNA) (Arnqvist *et al.*, 2010; Ballard and Rand, 2005; Kurbalija *et al*., 2014; Martin, 1995), and interactions between genomes and environment are involved in determining metabolism (Hoekstra *et al.*, 2013; Hoekstra *et al.*, 2018).

Energy balance is particularly keen in holometabolous species where larval development and growth tends to be rapid and massive, requiring simultaneous accumulation of the resources needed to fuel metamorphosis and emergence as a reproductive adult. *Drosophila melanogaster* is an especially powerful system to study developmental metabolism, given the genetic resources and an approximately 200-fold increase in body mass across three larval instars (Church and Robertson, 1966). There is evidence of significant genetic variation for metabolic rate within *Drosophila* species (Montooth *et al.*, 2003; Hoekstra *et al.*, 2013), and mitochondrial–nuclear genotypes that disrupt mitochondrial function also adversely affect larval metabolic and development rates (Meiklejohn *et al.*, 2013; Hoekstra *et al.*, 2013). Transcriptomic and metabolic

profiling in *D. melanogaster* indicate the dynamic nature of energy homeostasis that draws on both aerobic and anaerobic energy production, as well as the presence of proliferative metabolic programs during larval development (Graveley *et al.*, 2011; Tennessen *et al.*, 2011). Despite this wealth of data, at present, we lack a detailed understanding of the links between genome variation, mitochondrial function and organismal metabolic rate during development in *Drosophila*.

In the present study, we tested whether metabolic strategies in *D. melanogaster* varied among genotypes and across larval instars for both wildtype and mitochondrial-nuclear genotypes that generate energetic inefficiencies. We found that there is significant variation for the ontogeny of metabolism at the level of mitochondrial aerobic capacity, but that this variation can be buffered at higher levels of metabolic performance via physiological homeostasis. In this way, we show that there may be multiple genotypic and physiological paths to equivalent organismal outcomes within populations.

Methods

Drosophila stocks and maintenance

We used four *Drosophila* mitochondrial-nuclear genotypes generated by Montooth *et al.*, 2010. The (*mtDNA*);*nuclear* genotype (*simw*^{501});*OreR* has a genetic incompatibility that decreases oxidative phosphorylation (OXPHOS) activity putatively via compromised mitochondrial protein translation, and disrupts larval metabolic rate, resulting in delayed development, decreased immune function, and reduced female fecundity (Meiklejohn *et al.*, 2013; Hoekstra *et al.*, 2013; Holmbeck *et al.*, 2015; Zhang *et al.*, 2017; Hoekstra *et al.*, 2018; Buchanan *et al.*, 2018). This mitochondrial-nuclear (hereafter referred to as mito-nuclear) incompatibility arises from an

epistatic interaction between naturally-occurring single nucleotide polymorphisms (SNPs) in the mt-tRNA^{Tyr} gene and the nuclear-encoded mt-tyrosyl-tRNA synthetase gene *Aatm* that aminoacylates this mitochondrial tRNA (Meiklejohn *et al.*, 2013). The other three genotypes – (*ore*);*OreR*, (*simw*^{501});*Aut*, and (*ore*);*Aut* – serve as wildtype genetic controls that enabled us to test for the effects of mitochondrial and nuclear genotypes, separately and interactively, on developmental physiology. Additionally, we measured traits in two inbred genotypes sampled in Vermont (*VT4* and *VT10*) as representatives of natural populations that were not manipulated to generate specific mito-nuclear genotypes.

All genotypes were raised on standard cornmeal-molasses-yeast *Drosophila* media and acclimated to 25°C with a 12 h:12 h dark:light cycle for at least three generations prior to all experiments. To collect first-, second- and third-instar larvae, adults were allowed to lay eggs for 3-4 hours on standard media, and larvae from these cohorts were staged based on developmental time and distinguishing morphological features.

Larval metabolic rate

Routine metabolic rate was measured as the rate of CO_2 produced by groups of twenty larvae of the same instar and genotype using a flow-through respirometry system (Sable Systems International, Henderson, NV) with established protocols (Hoekstra *et al.*, 2013). Groups of larvae were collected onto the cap of 1.7 mL tube containing 0.5 mL of fly media and placed inside one of four respirometry chambers that were housed in a temperature-controlled cabinet (Tritech™ Research, Los Angeles, CA) maintained at 25°C. Between 8 and 13 biological replicates for each genotype and instar were randomized across chambers and respirometry runs, during which each group of larvae was sampled for CO_2 production for two, ten-minute periods.

149 CO_2 that accumulated in the chambers as a result of larval metabolism was detected using an
150 infrared CO_2 analyzer (Li-Cor 7000 CO_2/H_2O Analyzer; LI-COR, Lincoln, NE). $\dot{V}CO_2$ was
151 calculated from the mean fractional increase in CO_2 at a constant air-flow rate of 100 ml/min
152 over a 10 min time interval for each replicate after baseline drift correction. The wet weight of
153 the group of larvae was recorded using a Cubis® microbalance (Sartorius AG, Göttingen,
154 Germany) at the beginning of each respirometry run.
155
156 *Isolation of Mitochondria*
157 Mitochondria were isolated from larvae following a protocol modified from Aw *et al.*, 2016.
158 100-200 larvae were collected and rinsed with larval wash buffer (0.7% NaCl and 0.1% Triton
159 X-100). Larvae were very gently homogenized in 300-500 µL of chilled isolation buffer (154
160 mM KCl, 1 mM EDTA, pH 7.4) in a glass-teflon Thomas® homogenizer on ice. The
161 homogenate was filtered through a nylon cloth into a clean chilled microcentrifuge tube. The
162 homogenate was then centrifuged at 1500g for 8 min at 4°C (Eppendorf Centrifuge 5810R). The
163 resulting mitochondrial pellet was suspended in 40-50 µL of ice-cold mitochondrial assay
164 solution (MAS: 15 mM KCl, 10 mM KH_2PO_4, 2 mM $MgCl_2$, 3 mM HEPES, 1 mM EGTA, FA-
165 free BSA 0.2%, pH 7.2). Unless otherwise stated, all chemicals were purchased from Sigma
166 Aldrich (St Louis, MO) or Fisher Scientific (Pittsburgh, PA) and were of reagent grade or higher.
167
168 *Mitochondrial Respiration*
169 Oxygen consumption of freshly isolated mitochondria was measured using the Oxygraph Plus
170 System (Hansatech Instruments, Norfolk, UK) in 3 mL water-jacketed glass chambers equipped
171 with a magnetic stirrer and Clark-type oxygen electrodes. Temperature of the respiration

chambers was kept constant at 25°C using a Fisher Isotemp® 4100 R20 refrigerated water circulator (Fisher Scientific, Hampton, NH). A two-point calibration of electrodes using air-saturated distilled water and sodium sulfite was done for establishing 100% and zero oxygen levels in the chamber, respectively. The assay was completed within 2 hours of mitochondrial isolation, and six or seven biological replicates were measured for each larval stage of each genotype. 50 µL (~1.5 mg protein) of mitochondrial suspension was added to 950 µL of MAS in the respiration chamber. Pyruvate (5mM) and malate (2.5mM) were used as respiratory substrates at saturating amounts. Maximum respiration (State 3) was achieved by adding 400 µM of ADP, and State 4^{+} respiration was calculated as described by Chance and Williams 1955 by adding 2.5 µg ml^{-1} oligomycin. Oligomycin is an ATPase inhibitor and State 4^{+} gives an estimate of oxygen consumption linked to mitochondrial proton leak, rather than to ATP production, at high membrane potential (Brand *et al.*, 1994). Uncoupled respiration (State 3u), indicative of maximum respiration or electron transport system (ETS) capacity, is achieved by adding 0.5 µM of carbonyl cyanide m-chlorophenyl hydrazone (CCCP). CCCP is a protonophore that increases proton permeability in mitochondria and effectively disconnects ETS from ATPase. Data were acquired and respiration rates were corrected for electrode drift using the OxyTrace^{+} software. The respiratory control ratio (RCR) was calculated as the ratio of State 3 over State 4^{+} (Estabrook 1967). Respiration rates were normalized by unit mitochondrial protein added. Protein concentrations were determined using Bio-Rad Protein Assay Dye Reagent Concentrate (Bio-Rad, 5000006) and bovine serum albumin (BSA) as a standard.

Mitochondrial membrane potential ($\Delta\Psi_m$)

Mitochondrial membrane potential was measured using the JC-1 indicator dye (Fisher Scientific, Hampton, NH) following a protocol modified from Villa-Cuesta *et al.*, 2014.100 mg of larvae were weighed and used to isolate mitochondria as described above. Approximately 1.4 mg of mitochondrial protein was added and the final volume was increased to 300 µL using MAS. 3 µL of a 1 µg/µL solution of JC-1 dissolved in dimethyl sulfoxide (DMSO) was added to the suspension. Mitochondrial samples were incubated for 30 min at 37°C protected from light. At the end of incubation, samples were centrifuged for 3 min at 6000g and suspended in 600 µL of fresh MAS. Mitochondrial membrane potential was expressed as the ratio of fluorescence for aggregate:monomeric forms of JC-1 at red (excitation 485 nm, emission 600 nm) and green (excitation 485 nm, emission 530 nm) wavelengths respectively. 50 µM of CCCP was added to collapse membrane potential as a negative control.

Citrate synthase activity

Citrate synthase activity was measured following the protocol from Meiklejohn *et al.*, 2013. 100-200 larvae were homogenized in 1 mL chilled isolation buffer (225 mM mannitol, 75 mM sucrose, 10 mM MOPS, 1 mM EGTA, 0.5% fatty acid-free BSA, pH 7.2) using a glass-teflon Thomas® homogenizer. The homogenate was centrifuged at 300g for 5 min at 4°C (Eppendorf Centrifuge 5810R). The supernatant was transferred into a clean tube and centrifuged again at 6000g for 10 min at 4°C. The resulting mitochondrial pellet was resuspended in 50 µL of respiration buffer (225 mM mannitol, 75 mM sucrose, 10 mM KCl, 10 mM Tris-HCl, and 5 mM KH_2PO_4, pH 7.2). All samples were stored at -80°C till further analysis.

Maximum citrate synthase activity (V_{max}) of the mitochondrial extracts was measured spectrophotometrically at 30°C using a Synergy 2 plate reader (BioTek, VT, USA). 6 µg of

mitochondrial protein was added to the assay mixture containing 100mM Tris-HCl (pH 8.0), 2.5 mM EDTA, 100 µM Acetyl Co-A and 100 µM of DTNB [5,5′-dithiobis (2-nitrobenzoic acid)]. The reaction was monitored for 2 min as a background reading. The reaction was then started by adding 500 µM oxaloacetate to the assay to generate CoA-SH. CoA-SH is then detected by its reaction with DTNB to form a yellow product (mercaptide ion) that was measured using absorbance at 412 nm. Enzyme activity was normalized by protein concentration of the sample added. Six biological samples per genotype and instar were measured, each with two technical replicates.

Lactate quantification

Whole-body lactate concentrations were measured by an NAD^+/NADH-linked fluorescent assay following the protocol of Callier *et al.*, 2015. 100-200 larvae were homogenized in 100-500 µL of 17.5% perchloric acid and centrifuged at 14,000g for 2 min at 4°C (Eppendorf Centrifuge 5810R). Following precipitation of proteins, the clear supernatant was transferred into a clean tube and neutralized with a buffer containing 2 M of KOH and 0.3 M of MOPS, and again centrifuged at 14,000g for 2 min at 4°C. 20-50 µL of neutralized sample was added to the assay buffer (pH 9.5) containing a final concentration of 1000 mM hydrazine, 100 mM Tris-base, 1.4 mM EDTA and 2.5 mM NAD^+ in a 96-well plate (Micro Flour® 1). The assay was performed in fluorescence mode (Ex/Em = 360/460 nm) using a Synergy H1 Hybrid Reader (BioTek, VT, USA). After incubating the plate at 5 min at room temperature, a background reading was taken. 17.5 U/well lactate dehydrogenase (Sigma L3916) diluted with Tris buffer was then added to each sample and the reaction mixture was allowed to incubate at 37°C for 30 min protected from light. A second reading was then taken to measure NADH levels, after correcting for background

fluorescence. Six biological samples per genotype and instar were measured, each with two technical replicates. Sodium lactate was used as a standard for the assay. Lactate concentrations in the samples were normalized by wet weight of the larvae.

Hydrogen peroxide (H_2O_2) quantification

100-200 larvae were weighed, rinsed with larval wash buffer (0.7% NaCl and 0.1% Triton X-100) and homogenized in 500 µL of pre-chilled assay buffer (pH 7.5) containing 20 mM HEPES, 100 mM KCl, 5% glycerol, 10 mM EDTA, 0.1% Triton X-100, 1 mM PMSF (Sigma P7626) and 1:10 (v/v) protease inhibitor cocktail (Sigma P2714) using a glass-teflon Thomas® homogenizer. The homogenate was centrifuged at 200g for 5 min at 4°C, and the supernatant was stored at -80°C. H_2O_2 concentration was determined with a fluorometric Hydrogen Peroxide (H_2O_2) Assay Kit (Sigma MAK 165) following the manufacturer's protocol in a 96-well plate (Micro Flour® 1) using the Synergy H1 Hybrid Reader (BioTek, VT, USA). Six biological samples per genotype and instar were measured, each with two technical replicates. H_2O_2 concentrations in the samples were expressed as nM/µg of protein.

Statistical analyses

All statistical analyses used the statistical package R version 2.15.1 (R Development Core Team 2011). We implemented standard major-axis regression in the R-package SMATR (Warton *et al.*, 2006; Hoekstra *et al.*, 2013) to estimate the relationship between log-transformed mass and $\dot{V}CO_2$, and to test for larval-instar and genetic effects on the slope of this relationship. When there was statistical evidence for a common slope among genotypes, we fit the common slope to test for effects of genotype on the y-intercept (i.e., genetic effects on the mass-specific metabolic

263 rate). We removed a single observation where a first-instar replicate had a $\dot{V}CO_2$ value less than
264 zero. Analysis of variance (ANOVA) was used to test for the fixed effects of mtDNA, nuclear
265 genome, larval instar, and all interactions on lactate accumulation, H_2O_2 concentration,
266 mitochondrial physiology (State3, State4, uncoupled respiration, RCR^+, and $\Delta\Psi_m$) and citrate
267 synthase activity in an ANOVA design. Post-hoc comparisons among instars within genotypes
268 and among genotypes within instar were evaluated using Tukey HSD tests.
269 *Data Availability*
270 Stocks and strains are available upon request. Supplemental files are available at FigShare.
271 Phenotypic data will be deposited in the Dryad Digital Repository upon publication.
272

273 **Results**

274 *Metabolic rate scaling with mass varies across larval instars and genotypes*
275 Metabolic rate scales with mass according to the power function $R = aM^b$, where a is the constant
276 scaling coefficient, M is mass, and b is the scaling exponent. The scaling exponent b, estimated
277 by the slope of the relationship between log-transformed metabolic rate and mass, differed
278 significantly across larval instars (Fig. 1A) ($LR = 18.1$, $df = 2$, $P = 0.0001$). Metabolic scaling
279 with body mass was hypermetric in first-instar larvae (b (CI) = 1.42 (1.21, 1.67)), isometric in
280 second-instar larvae (b = 1.04 (0.95, 1.15)), and hypometric in third-instar larvae (b = 0.85 (0.71,
281 1.01)). Within first- and second-instar larvae, there was no evidence that metabolic scaling with
282 mass differed significantly among genotypes, nor were there significant effects of genotype on
283 the elevation of the fitted relationship (i.e., on the mass-specific metabolic rate) (Fig. 1B, 1C and
284 Table 1). However, there was more variance among genotypes in mass-specific metabolic rate in
285 first-instar larvae relative to second-instar larvae (Fig. 1B, 1C and Table 1). Metabolic scaling

with mass in third-instar larvae differed significantly among genotypes, as evidenced by significantly different slopes (Fig. 1D and Table 1). The variation in metabolic scaling with mass did not result from natural lines differing from mito-nuclear genotypes, but rather from variation in the scaling exponent within both sets of genotypes. The pattern was significant regardless of the inclusion of several data points that, while not statistical outliers, did appear as outliers in the relationship between metabolic rate and mass (Fig. 1D and Supplemental Table 1).

Mitochondrial respiration is similar across larval instars and genotypes

Despite these ontogenetic and genetic differences in the scaling of organismal metabolic rate with mass, second- and third-instar larvae had similar rates of mitochondrial oxygen consumption linked to ATP production (i.e., State 3 respiration) per unit of mitochondrial protein in both mito-nuclear genotypes (*instar*, $P = 0.13$) and natural genotypes (*instar*, $P = 0.12$) (Fig. 2) (Supplemental Table 2). State 3 respiration from first-instar larvae mitochondrial preparations were either below our detection limits or of low-quality, even when including similar amounts of larval mass in the preparation. This indicates that there is likely an increase in mitochondrial quantity or functional capacity between the first- and second-larval instars. Furthermore, State 3 respiration did not differ significantly among mito-nuclear or natural genotypes, nor were there any significant interactions between instar and genetic factors (Supplemental Table 2). Maximum respiratory capacity of mitochondria (or CCCP- induced uncoupled respiration) was also maintained across instars in all mito-nuclear genotypes (*instar*, $P= 0.18$) (Supplemental Fig. 1A and Supplemental Table 2). However, the natural genotype *VT10* had a significantly elevated maximal respiratory capacity in the second instar that resulted in a significant instar-by-genotype interaction ($P= 0.001$) (Supplemental Fig. 1A and Supplemental Table 2).

Healthy mitochondria have high rates of oxygen consumption and ATP production when ADP is abundant (i.e., State 3 respiration), but low rates of oxygen consumption in the absence of ATP synthesis (i.e., State 4^+ respiration). The ratio of these two measures is called the respiratory control ratio (RCR^+). While the RCR^+ was generally maintained at a ratio of 2-3 across genotypes and instars, two genotypes, (*ore*);*OreR* and *VT10,* had elevated RCR in third-instar larvae that contributed to a significant instar-by-genotype interaction in both mito-nuclear (instar x nuclear, $P = 0.004$) and natural genotypes (instar x genotype, $P = 0.0001$) (Supplemental Fig. 1B and Supplemental Table 2). This was due to decreased State 4^+ respiration in second-instar mitochondria from these genotypes (Supplemental Fig. 1C and Supplemental Table 2).

Certain genotypes use anaerobic ATP production further into development

We measured the activity of citrate synthase, a nuclear-encoded enzyme located in the mitochondrial matrix. As the first step in the Tricarboxylic Acid (TCA) cycle, the activity of this enzyme is often used as an indicator of cellular oxidative capacity. Citrate synthase activity per unit of mitochondrial protein increased across development in all genotypes (Fig. 3) (mito-nuclear genotypes: instar, $P< 0.0001$; natural genotypes: instar, $P < 0.0001$). There were also genotype-specific effects on citrate synthase activity. The energetically compromised (*simw*^{501});*OreR* genotype had elevated citrate synthase activity relative to other genotypes across all three instars (Fig. 3), resulting in significant epistatic mito-nuclear variance for this measure of oxidative capacity (mito x nuclear, $P = 0.022$) (Supplemental Table 3). Genotype-by-instar interactions significantly affected citrate synthase activity in the natural genotypes (instar x genotype, $P = 0.010$). Genotypes could be categorized as those for which citrate synthase reaches

is maximal level by the second instar (e.g., *VT10* and (*ore*);*Aut*) and those for which second-instar mitochondria have citrate synthase activity levels intermediate to first- and third-instar mitochondria (e.g., *VT4* and *(ore)*;*OreR*) (Fig. 3).

In addition to aerobic, oxidative ATP production, *D. melanogaster* larvae use anaerobic, glycolytic ATP production that results in the production of lactate. There was significant genetic variation in the extent to which larvae accumulated lactate during development. Second-instar larvae of some genotypes significantly accumulated lactate, while others genotypes did not accumulate any lactate across development (Fig. 4A). This pattern was observed in both the mito-nuclear genotypes (instar x mtDNA x nuclear, $P = 0.033$) as well as in the natural genotypes (instar x genotype, $P = 0.009$). The energetically compromised ($simw^{501}$);*OreR* genotype accumulated the highest amounts of lactate in the second instar, relative to other genotypes, resulting in a strong mito-nuclear interaction (Fig. 4B and Supplemental Table 4). However, the natural genotype *VT4* also accumulated high levels of lactate in second-instar larvae (Fig. 4A). Furthermore, genotypes that had intermediate levels of citrate synthase activity during the second instar (e.g., *VT4* and *(ore)*;*OreR*) also tended to have increased lactate accumulation during the second instar.

The mito-nuclear incompatible genotype accumulates more ROS and has lower mitochondrial membrane potential

All genotypes had significantly increased levels of H_2O_2 by the third instar, relative to earlier instars ($P < 0.0001$) (Fig. 5A and Supplemental Table 5). However, the energetically-compromised ($simw^{501}$);*OreR* genotype had significantly elevated levels of H_2O_2 in the second instar, both relative to other genotypes and to first- and third-instars of the same genotype. This

355 resulted in a significant effect of the instar x mtDNA x nuclear interaction on levels of H_2O_2 ($P <$
356 0.0001) (Fig. 5B and Supplemental Table 5).

357 Because mitochondrial membrane potential ($\Delta\Psi_m$) provides the driving force that is utilized
358 by ATP synthase (complex V of OXPHOS) to make ATP and is used as an indicator of
359 mitochondrial viability and cellular health, we tested whether this was disrupted in
360 (*simw*^{501});*OreR*. All genotypes, except (*simw*^{501});*OreR*, maintained high levels of mitochondrial
361 membrane potential in second- and third-instar larvae (Fig. 6A and Supplemental Table 6). The
362 energetically-compromised (*simw*^{501});*OreR* genotype had significantly lower mitochondrial
363 membrane potential relative to other genotypes in both second- and third-instar larvae. The effect
364 of the mito-nuclear interaction on this marker of mitochondrial and cellular health was
365 particularly pronounced in the second instar (instar x mtDNA x nuclear $P < 0.0001$) (Fig. 6B and
366 Supplemental Table 6).

367 In summary, the maintenance of mitochondrial respiration in the energetically compromised
368 (*simw*^{501});*OreR* genotype across second and third instars was coincident with significant
369 increases in oxidative capacity of mitochondria, increased lactate and ROS production during the
370 second instar, and decreased mitochondrial membrane potential.

371

372 **Discussion**

373 *Ontogenetic shifts in the relationship between metabolic rate and mass*

374 Metabolic rates scale allometrically with mass, but the parameters that define this
375 relationship vary among taxa, genotypes, life stages and environments (Glazier, 2005; Greenlee
376 *et al.*, 2014). We found that the relationship between mass and metabolic rate differed
377 significantly among larval instars of *D. melanogaster*. Metabolic scaling in developing animals

has been described as an “impasse of principles," wherein the basic tenant of metabolic allometry—that the physiological principles of organisms are relatively conserved—is at odds with the basic tenant of development—that the physiological state of organisms is dynamic across ontogeny (Burggren, 2005). Insect development involves complex changes in cellular energy demand and body composition that likely affect how metabolic rate scales with mass. Thus, models and principles of interspecific allometric scaling may not be applicable to ontogenetic scaling.

We observed a shift from hypermetric scaling in first-instar larvae (b>1), to isometric allometry in second-instar larvae (b=1), followed by hypometric allometry in third-instar larvae (b<1). The shift in metabolic scaling towards lower mass-specific metabolic rates in larger instars, was in spite of our observation that larger instars had seemingly greater capacity for oxygen-dependent ATP production, as indicated by increased levels of citrate synthase activity per unit of mitochondria. Nevertheless, mitochondrial oxygen consumption linked to ATP production was maintained at similar levels across second- and third-instar larvae. These patterns suggest that although there may be increased oxidative capacity of mitochondria as development progresses, mitochondrial respiration and organismal respiration are not simple reflections of oxidative capacity, but rather are emergent properties of organellar, cellular and organismal processes.

The ontogenetic change in metabolic scaling that we observed may reflect a change in energy demand across development as larval growth transitions from cell proliferation to cell growth. Hypermetric metabolic scaling exponents (b>1), where metabolic rates of larger individuals are greater per unit mass, could result from the increased energetic costs associated with the rapid cell proliferation and increase in cell number early in *Drosophila* development (O’Farrell, 2004;

Vollmer *et al.*, 2017). Later in development, larval accumulation of mass occurs primarily via increases in cell volume (O'Farrell, 2004), reducing the surface area to volume ratio of cells and potentially limiting metabolism. These observations support studies, collectively grouped under Resource Demand (RD) models, that suggest that metabolic scaling is driven by an intrinsic metabolic demand from the cellular level to tissue growth potential (VonBertalanffy and Pirozynski, 1953; Shin and Yasuo, 1984, 1993; Ricklefs, 2003; Glazier, 2005). In this way, an organism's metabolic rate (and by extension metabolic scaling) across development is a reflection of the potential of tissues for proliferation and growth (Ricklefs, 2003). Our observations also contribute to a small, but growing number of insect studies that support a conceptual framework for patterns of intraspecific ontogenetic scaling where completion of growth in holometabolous insects is correlated with decreased mass-specific metabolic rates (Glazier, 2005). In both the tobacco hornworm *Manduca sexta,* and the silkworm *Bombyx mori*, metabolic scaling exponents also decrease across ontogeny (Blossman-Myer and Burggren, 2010; Callier and Nijhout, 2011, 2012; Sears *et al.*, 2012).

Metabolic scaling with mass may also be influenced by the biochemical composition of the body. System Composition (SC) models hypothesize that ontogenetic changes in metabolic scaling reflect shifts in body composition and the relative proportions of metabolically active versus inert or "sluggish" tissues (Glazier, 2005; Isler and VanSchaik, 2006; Greenlee *et al.*, 2014). Tissue lipid composition and lipid storage change across development in *Drosophila*, with a net increase of metabolically-inert storage lipids like triacylglycerides across development (Carvalho *et al.*, 2012). The increased contribution of less metabolically active tissue to the body could also contribute to the observed developmental shift from hypermetric to hypometric metabolic scaling. In *Manduca*, the contribution of metabolically active gut tissue to the body

424 decreases across development, which may contribute to an increasingly hypometric metabolic
425 scaling with mass across development (Callier and Nijhout, 2012).

426 Genetic variation in body composition across development could also underlie the significant
427 genetic variation in metabolic scaling that we observed in third-instar larvae. If genotypes differ
428 in the degree to which they accumulate mass in the third instar via different types of energy
429 storage, this could generate genetic variation for how metabolic rate scales with mass. Midway
430 through the third instar, *D. melanogaster* membrane-lipid accumulation is paused, while levels of
431 storage lipids like triacylglycerides increase (Carvalho *et al.*, 2012).This suggests a transition in
432 the third instar from metabolism supporting membrane synthesis and cell proliferation to
433 metabolism supporting mass accumulation via lipid storage. If genotypes vary in the timing or
434 extent of this switch, as we have seen for mitochondrial metabolism (described below), this
435 could contribute to the greater genetic variation for metabolic rate and scaling that we observed
436 in this developmental stage.

437

438 *Genetic variation in cellular metabolism may support similar organismal outcomes*

439 Aerobic organisms can generate ATP via mitochondrial OXPHOS, but also anaerobically
440 via glycolytic pathways that are supported by fermentation-generated NAD^+ (e.g., by lactate
441 production). We observed a consistent pattern across genotypes of increased oxidative capacity
442 to aerobically produce ATP across development, consistent with a metabolic switch from
443 glycolytic to mitochondrial production of ATP regulated by the *Drosophila* estrogen-related
444 receptor *dERR* (Tennessen *et al*., 2011; Tennessen and Thummel, 2011). However, genotypes
445 differentiated into two categories of metabolic phenotypes—those that appeared to switch to
446 mitochondrial ATP production before the second instar and accumulated very little lactate, and

447 those that appeared to rely on glycolytic ATP production with significant lactate accumulation
448 during the second instar. Yet, despite this genetic variation in how second-instar larvae were
449 generating ATP, the organismal metabolic rate of second-instar larvae was more robust to
450 genetic variation than were the metabolic rates of other instars. We also observed that despite
451 this developmental switch from glycolytic to mitochondrial ATP production, *in vitro*
452 mitochondrial respiration rates per unit mitochondrial protein remained constant across second-
453 and third-instar larvae. Again, this highlights that organellar and organismal metabolic rates
454 emerge from cellular, tissue and organismal-level processes, and are not simple reflections of the
455 underlying metabolic pathways being used. In this way, higher levels of biological organization
456 may buffer and potentially shelter genetic variation in metabolism from selection.

457 Using glycolytic ATP production may seem counterintuitive and less efficient than oxidative
458 ATP production. However, glycolytic ATP production may provide several developmental
459 advantages. First, it meets the bioenergetic needs of growth by providing abundant ATP. Despite
460 the low yield of ATP per glucose consumed, the percentage of total cellular ATP produced from
461 glycolysis can exceed that produced by OXPHOS (Lunt and Vander-Heiden, 2011). Second,
462 there are reports of moonlighting functions of glycolytic enzymes translocating to the nucleus
463 where they act as transcription factors to promote proliferation (Marden, 2013; Lincet and Icard,
464 2014; Boukouris *et al.*, 2016). Third, glycolytic ATP production enables flux through the pentose
465 phosphate and TCA pathways to provide carbon-backbone intermediates for building
466 macromolecules such as ribose sugars for DNA, amino acids for proteins, glycerol and citrate for
467 lipids, as well as reducing power to support cell proliferation and growth during development
468 (Tennessen *et al.*, 2011, 2014; Tennessen and Thummel, 2011; Lunt and Vander-Heiden, 2011).

469 *dERR* is responsible for a vital transcriptional switch of carbohydrate metabolism in second-
470 instar larvae (Tennessen *et al.*, 2011) that coincides with increases in lactate dehydrogenase
471 (*dLDH*) and lactate accumulation (Li *et al.*, 2017). dLDH activity recycles NAD^+ which allows
472 for continued glycolytic ATP production and supports the TCA cycle in generating cellular
473 building blocks. Furthermore, dLDH expression and lactate production results in the
474 accumulation of the metabolic signaling molecule L-2-hydroxyglutarate that affects genome-
475 wide DNA methylation and promotes cellular proliferation (Li *et al.*, 2017). We found that
476 second-instar lactate accumulation was strongly affected by genotype, suggesting differential
477 timing of this switch among both wild-type and mito-nuclear genotypes. Investigating potential
478 bioenergetics and life-history consequences of this genetic variation may reveal whether
479 different metabolic strategies at the sub-cellular level fund similar or distinct fitness outcomes at
480 the organismal level. This is critical for understanding whether populations harbor genetic
481 variation in biochemical pathways that ultimately has similar fitness outcomes or whether we
482 should expect to see the signatures of selection acting on enzymes that control shifts in metabolic
483 flux (e.g., Flowers *et al*., 2007; Pekny *et al*., 2018).
484
485 *Physiological compensation in a mito-nuclear incompatible genotype comes at a cost*
486 Mitochondrial respiration coupled to ATP production was maintained in the mito-nuclear
487 incompatible genotype at *in vitro* levels similar to control genotypes, despite compromised
488 OXPHOS via a presumed defect in mitochondrial protein synthesis in this genotype (Meiklejohn
489 *et al*., 2013). The maintenance of mitochondrial respiration in this genotype was accompanied by
490 increases in mitochondrial oxidative capacity, measured by citrate synthase activity, and
491 glycolytic ATP production, measured by lactate accumulation, relative to control genotypes.

These increases may reflect physiological compensation to maintain ATP levels in a genotype whose mitochondria consume similar levels of oxygen but are less efficiently generating ATP. We suggest that by using the functional complementation of both glycolytic and mitochondrial ATP production, this genotype is able to synthesize the ATP needed to support its development.

Physiological compensation can have diverse and sometimes counter-intuitive costs paid over the lifespan that can adversely affect fitness. While (*sim*^{w501}); *OreR* appears able to physiologically compensate to survive larval development, this genotype has delayed development and compromised pupation height, immune function and female fecundity (Meiklejohn *et al*., 2013; Zhang *et al*., 2017; Buchanan *et al*., 2018). Additionally, while *in vitro* mitochondrial respiration in this genotype was maintained similar to other genotypes, larval metabolic rate in this genotype was elevated, potentially via compensatory upregulation of aerobic capacity to supply ATP (Hoekstra *et al*., 2013). Thus, even when drawing on both glycolytic and oxidative ATP production, individuals with this mito-nuclear incompatibility may produce energy supplies very close to demand during larval growth. Previous results from our lab support this model; when development of (*sim*^{w501}); *OreR* was empirically accelerated, development and reproduction were even more compromised, suggesting that this genotype has limited capacity to compensate the defect in OXPHOS (Hoekstra *et al.*, 2013, 2018). This genotype may use all of its aerobic scope to complete normal development compared to the other genotypes, leaving few resources leftover for other aspects of fitness. Once the demands of growth are removed, this genotype appears to regain some aerobic scope, as larvae that survived to pupation also completed metamorphosis and had normal adult size and metabolic rates (Hoekstra *et al.*, 2013, 2018). However, the costs paid out during development appear to have significant impacts on adult fecundity. Both female and male fecundity were severely

515 compromised in this genotype when development occurred at warmer temperatures that increase
516 biological rates and energy demand (Hoekstra *et al.*, 2013; Zhang *et al.*, 2017).
517 At the cellular level, physiological compensation in (sim^{w501}); *OreR* larvae may be a source
518 of oxidative stress, indicated by higher levels of H_2O_2, relative to other genotypes. H_2O_2 is a
519 byproduct of the mitochondrial electron transport system (ETS) that supports OXPHOS in
520 healthy cells, and we observed increases in H_2O_2 as oxidative capacity increased across
521 development in all genotypes. However, compromised electron flow through the ETS can
522 increase H_2O_2 levels and generate oxidative stress (Somero *et al.*, 2017). There are two ways that
523 this may be occurring in (sim^{w501}); *OreR* mitochondria. First, upregulation of the TCA cycle to
524 supply more NADH for ATP production via the ETS may increase production of superoxide
525 anion at Complex I. Second, there may be stoichiometric imbalance in the ETS due to
526 presumably normal levels of cytoplasmically-translated Complex II but compromised levels of
527 the mitochondrially-translated downstream OXPHOS complexes in this genotype. This could
528 result in backflow of electrons that can produce superoxide ions when the ratio of
529 reduced:unreduced coenzyme Q become elevated. The idea that (sim^{w501}); *OreR* individuals are
530 experiencing oxidative stress suggests an alternative interpretation of the elevated citrate
531 synthase activity that we observed in this genotype. Levels of citrate synthase were increased in
532 the blue mussel *Mytilus trossulus* in response to heat stress, a change that was coupled with
533 increases in isocitrate dehydrogenase (IDH), which generates $NADPH^+$ to support H_2O_2-
534 scavenging reactions in the mitochondria (Tomanek and Zuzow, 2010). This highlights the
535 importance of considering that TCA cycle enzymes provide important functions beyond their
536 role in OXPHOS, as they provide substrates for biosynthesis, support antioxidant reactions, and
537 act as signaling molecules (Marden, 2013; Boukouris *et al.*, 2016; Somero *et al.*, 2017).

538 Finally, we observed that (sim^{w501}); *OreR* mitochondria could support mitochondrial oxygen
539 consumption linked to ATP production at wild-type levels despite the fact that their membrane
540 potential was significantly reduced. There is precedence for this observation. For example,
541 mitochondrial diseases with OXPHOS defects are correlated with a suite of metabolic
542 phenotypes that include upregulated glycolysis, lactate accumulation, elevated ROS, and
543 decreased mitochondrial membrane potential, but stable ATP levels (Szczepanowska *et al.*,
544 2012; Frazier *et al.*, 2017). ROS act as essential secondary messengers in cellular homeostasis,
545 but above a certain threshold level can be dangerous and lead to apoptosis (Giorgio *et al.*, 2007;
546 Bigarella *et al.*, 2014). A potential regulatory and defense mechanism is to decrease the
547 mitochondrial membrane potential (e.g., by uncoupling) to reduce further ROS production and
548 protect the cell from oxidative damage (Dlasková *et al.*, 2006). Our data cannot distinguish in
549 this mito-nuclear genotype whether upregulation of citrate synthase and decreased membrane
550 potential in the mitochondria are the cause or the consequence of oxidative stress. However, new
551 models from ecophysiology (Tomanek and Zuzow 2010), developmental physiological genetic
552 (Tennessen *et al.* 2011, 2014; Li *et al.* 2017) and disease (Ward and Thompson 2012) systems
553 provide promising paths for future elucidation of the mechanisms by which mitochondrial-
554 nuclear genetic variation scales up to organismal fitness variation.
555 In conclusion, the dramatic and rapid growth of *Drosophila* during ontogeny requires a
556 precise and genetically determined metabolic program that enhances biosynthesis and
557 proliferation coupled with a tight temporal coordination. Here, we have shown how genetic
558 variation influence patterns of metabolism in both natural and mito-nuclear genotypes of
559 *Drosophila* during its developmental progression. Our study reveals that genetic defects in core
560 physiology can be buffered at the organismal level via physiological compensation and that

natural populations likely harbor genetic variation for distinct metabolic strategies in development that generate similar organismal outcomes.

Acknowledgements and funding

We would like to thank Madeleine Koenig who was supported by the Undergraduate Creative Activities and Research Experience (UCARE) program at UNL for her assistance with sample preparation. The research was supported by NSF-IOS CAREER Award 1149178, NSF EPSCoR Track II Award 1736249 , and funds from the University of Nebraska-Lincoln to OBM, CRJ and KLM.

Table 1. Genetic effects on routine metabolic rate (RMR) as a function of mass across developmental instars

Phenotype	Genotype	Slope (95% CI)[1]	Y-intercept[2]
First-instar RMR		H_0: equal slopes (*LR*=4.61,*df*=5,*P*=0.46)	H_0: no elevation difference (*Wald*=9.28,*df*=5,*P*=0.10)
	Common slope	1.29 (1.10,1.54)	
	VT10		0.66 (0.54,0.77)
	VT4		0.75 (0.64,0.86)
	(*ore*);*Aut*		0.62 (0.51,0.73)
	(*ore*);*OreR*		0.61 (0.43,0.79)
	(*simw*^{501});*Aut*		0.50 (0.26,0.75)
	(*simw*^{501});*OreR*		0.59 (0.42, 0.75)
Second-instar RMR		H_0: equal slopes (*LR*=3.99,*df*=5,*P*=0.55)	H_0: no elevation difference (*Wald*=2.58,*df*=5,*P*=0.76)
	Common slope	1.01 (0.90,1.13)	
	VT10		0.65 (0.55,0.75)
	VT4		0.71 (0.6,0.81)
	(*ore*);*Aut*		0.67 (0.58,0.75)
	(*ore*);*OreR*		0.62 (0.51,0.73)
	(*simw*^{501});*Aut*		0.67 (0.55,0.79)
	(*simw*^{501});*OreR*		0.67 (0.57,0.76)
Third-instar RMR		H_0: equal slopes (*LR*=20.1,*df*=5,*P*=**0.001**)	
	VT10	1.16 (0.65,2.06)	
	VT4	0.78 (0.54,1.10)	
	(*ore*);*Aut*	0.81 (0.65,1.00)	
	(*ore*);*OreR*	1.00 (0.81,1.24)	
	(*simw*^{501});*Aut*	0.36 (0.25,0.52)	
	(*simw*^{501});*OreR*	0.41 (0.19,0.89)	

[1] Either a common or genotype-specific slope with confidence interval, when justified by the test for equal slopes among genotypes.

[2] In no case was there evidence that there was a shift in mass along the x-axis among genotypes ($P > 0.09$).

576
577

578 **Figure legends**

579 Figure 1. Metabolic scaling with mass varied across larval development and among genotypes.
580 A) The mass-scaling exponent for routine metabolic rate ($\dot{V}CO_2$) differed significantly among
581 instars ($LR = 18.1$, $df = 2$, $P = 0.0001$), with the relationship between metabolic rate and mass
582 becoming more shallow across development. B,C) There was more genetic variation for
583 metabolic rate in first-instar larvae, relative to second-instar larvae. D) Mass-scaling exponents
584 differed significantly among genotypes in the third instar of development (Table 1 and
585 Supplemental Table 1).
586
587 Figure 2. Oxygen-coupled ATP production, measured by the State 3 mitochondrial oxygen
588 consumption per unit of mitochondrial protein, was maintained at statistically similar levels
589 across genotypes and instars (Supplemental Table 2).
590
591 Figure 3. Oxidative capacity, measured by citrate synthase activity (V_{max}) per unit of
592 mitochondrial protein, increased significantly across instars and was largest in the energetically-
593 compromised (*simw*^{501});*OreR* genotype. A) While all mito-nuclear genotypes increased oxidative
594 capacity throughout development, there was significant variation among genotypes.
595 (*simw*^{501});*OreR* larvae had significantly higher oxidative capacity than its nuclear genetic control
596 (*ore*);*OreR* in the second ($*P_{Tukey's} = 0.015$) and third instars ($**P_{Tukey's} = 0.008$). The *simw*^{501}
597 mtDNA had no effect in the *Aut* background ($P_{Tukey's} > 0.833$ in both instars), resulting in a
598 significant mtDNA x nuclear interaction ($P = 0.022$). Wild-type genotypes from Vermont also
599 varied significantly in the extent to which oxidative capacity reached its maximal level in the
600 second versus third instar of development (Supplemental Table 3). Different letters within

601 genotypes denote significantly different means at $P_{Tukey's} < 0.006$, and asterisks designate
602 significant differences between genotypes of the same larval instar.
603
604 Figure 4. A) Lactate levels per gram of larvae, varied significantly among genotypes in second-
605 instar larvae and was highest in the energetically-compromised (*simw*^{501});*OreR* genotype.
606 Genetic variation for second-instar larval lactate levels was also observed among wild-type
607 genotypes from Vermont (instar x genotype, $P = 0.009$) (Supplemental Table 4), with *VT4*
608 having significantly more lactate than *VT10* (**$P_{Tukey's} = 0.014$). B) There was a significant instar
609 x mtDNA x nuclear interaction effect on lactate levels ($P = 0.033$) (Supplemental Table 4).
610 (*simw*^{501});*OreR* larvae had significantly higher lactate levels than all other genotypes in the
611 second instar (*$P_{Tukey's} < 0.015$). B) Different letters within genotypes denote significantly
612 different means at $P_{Tukey's} < 0.036$, and asterisks designate significant differences between
613 genotypes of the same larval instar.
614
615 Figure 5. A) ROS levels, measured as the concentration of H_2O_2 per gram of larvae, increased
616 significantly across instars, and were highest in second-instar larvae of the energetically-
617 compromised (*simw*^{501});*OreR* genotype. B) There was a strong effect of instar on ROS levels
618 (instar, $P = 2.347e\text{-}12$), but this pattern varied among mito-nuclear genotypes (instar x mtDNA x
619 nuclear, $P = 5.166e\text{-}05$) (Supplemental Table 5). Second-instar (*simw*^{501});*OreR* larvae had
620 significantly higher ROS levels relative to all other genotypes (***$P_{Tukey's} < 0.0001$), while all
621 other genotypes had similar patterns of increasing ROS throughout development. The interaction
622 between instar and genotype did not affect ROS levels among wild-type genotypes
623 (Supplemental Table 5), which had a similar pattern to the control mito-nuclear genotypes.

624 Different letters within genotypes denote significantly different means at $P_{Tukey's} < 0.041$, and
625 asterisks designate significant differences between genotypes of the same larval instar.
626
627 Figure 6. The energetically compromised (*simw*^{501});*OreR* genotype had significantly decreased
628 mitochondrial quality, as measured by the mitochondrial membrane potential ($\Delta\Psi_m$). A) Both
629 mito-nuclear and wild-type genotypes from Vermont generally maintained high membrane
630 potential in second- and third-instar larvae. However, (*simw*^{501});*OreR* larvae had significantly
631 lower mitochondrial membrane potential than the nuclear genetic control (*ore*);*OreR* in the
632 second (***$P_{Tukey's} < 0.0001$) and third instars (*$P_{Tukey's} = 0.016$). B) This effect of the *simw*^{501}
633 mtDNA was not evident in the *Aut* background, where it increased membrane potential in
634 second-instar larvae and had no effect in third-instar larvae ($P_{Tukey's} = 0.167$). This resulted in a
635 significant effect of an instar x mito x nuclear interaction (P = 1.580e-05) (Supplemental Table
636 6). Values above 2 typically indicate healthy mitochondria. Different letters within genotypes
637 denote significantly different means at $P_{Tukey's} < 0.002$, and asterisks designate significant
638 differences between genotypes of the same larval instar.

639 **Figure 1.** Larval metabolic rate

640

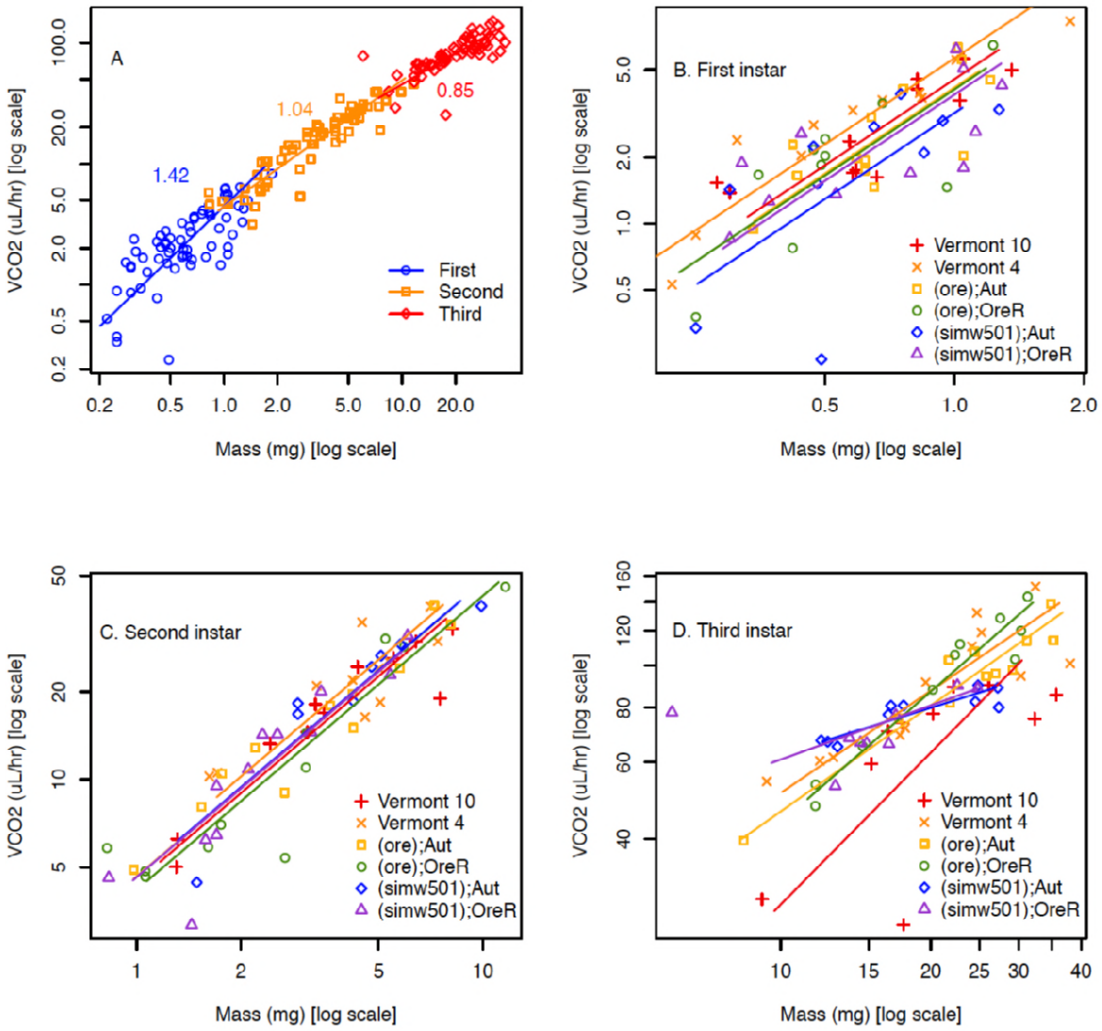

641

642 **Figure 2.** State 3 mitochondrial O_2 consumption

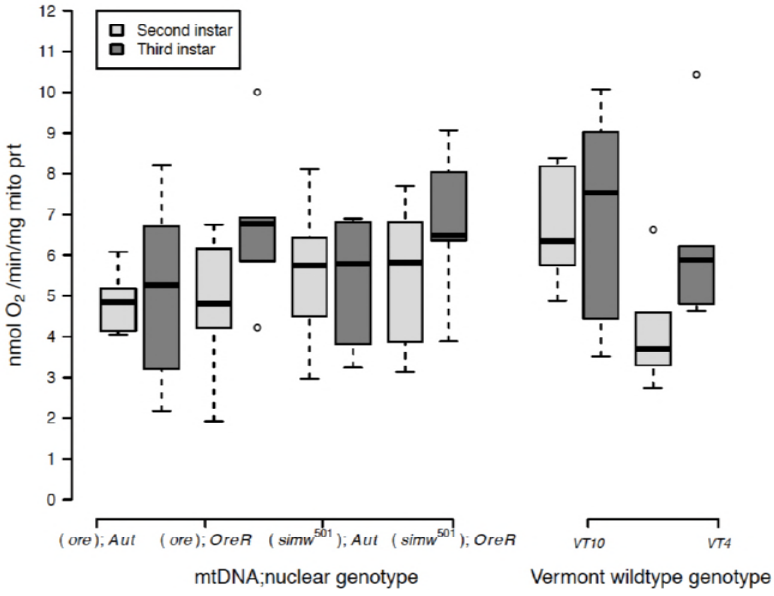

643

644 **Figure 3.** Citrate synthase activity

645

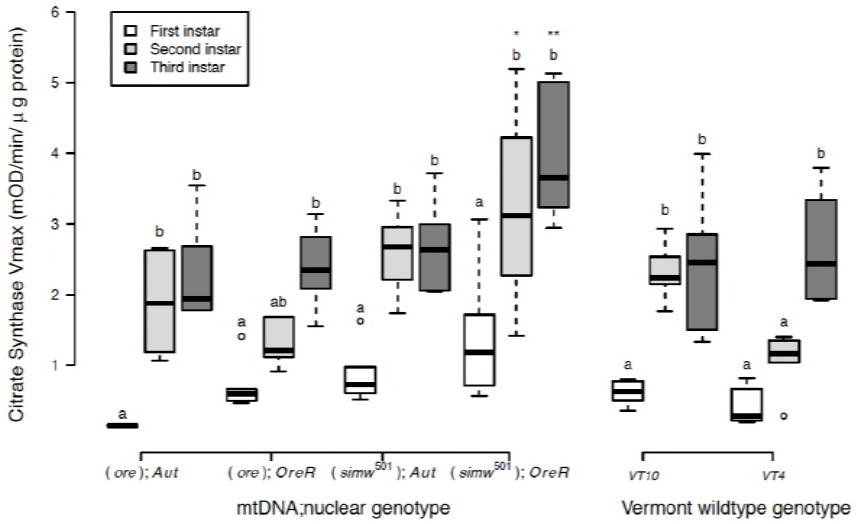

646

Figure 4. Lactate accumulation

A. **B.**

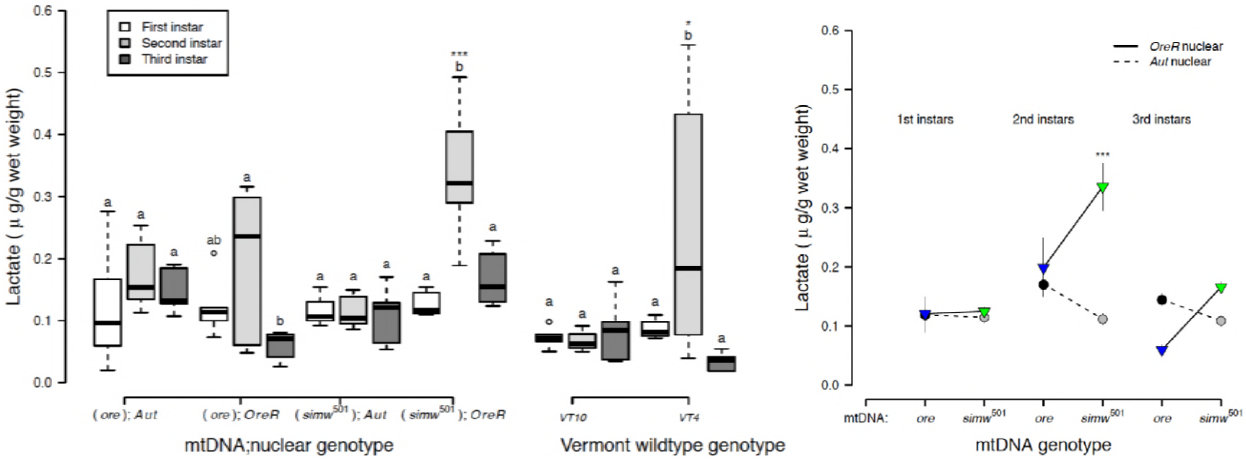

Figure 5. Reactive oxygen species (H_2O_2)

A. **B.**

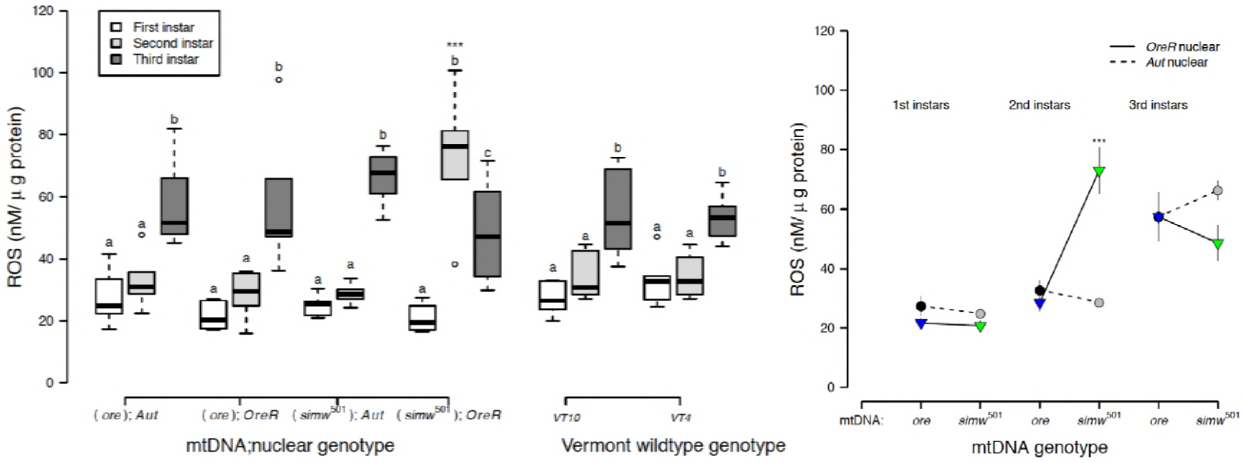

Figure 6. Mitochondrial membrane potential ($\Delta\Psi_m$)

A. **B.**

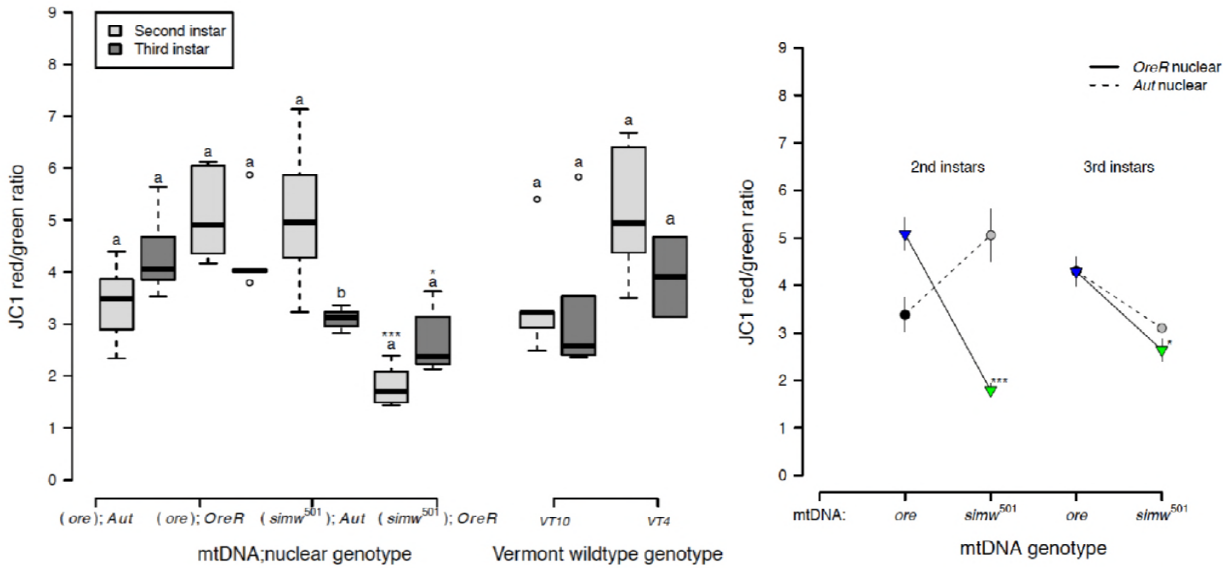

Literature Cited

Arnqvist G., Dowling D., Paul E., Laurene G., Tom T., *et al*., 2010 Genetic architecture of metabolic rate: environment specific epistasis between mitochondrial and nuclear genes in an insect. Evolution. 64: 3354–3363.

Aw W., Bajracharya R., Towarnicki S., Ballard J., 2016 Assessing bioenergetic functions from isolated mitochondria in *Drosophila melanogaster*. J. Biol. Methods. 3: e42.

Ballard W., Rand D., 2005 The population biology of mitochondrial DNA and its phylogenetic implications. Annu. Rev. Ecol. Evol. Syst. 36: 621–642.

Barabási A., Oltvai Z., 2004 Network biology: understanding the cell's functional organization. Nat. Rev. Genet. 5: 101.

Bigarella C., Liang R., Ghaffari S., 2014 Stem cells and the impact of ROS signaling. Development 141: 4206 -4218.

Blossman-Myer B., Burggren W., 2010 Metabolic allometry during development and metamorphosis of the silkworm *Bombyx mori*: analyses, patterns, and mechanisms. Physiol. Biochem. Zool. 83: 215–231.

Boukouris A., Zervopoulos S., Michelakis E., 2016 Metabolic enzymes moonlighting in the nucleus: metabolic regulation of gene transcription. Trends Biochem. Sci. 41: 712–730.

Brand M., Chien L., Ainscow E., Rolfe D., Porter R., 1994 The causes and functions of mitochondrial proton leak. Biochim. Biophys. Acta - Bioenerg. 1187: 132–139.

Buchanan J., Meiklejohn C., Montooth K., 2018 Mitochondrial dysfunction and infection generate immunity-fecundity tradeoffs in *Drosophila*. Integr. Comp. Biol. 58: 591-603.

Burggren W., 2005 Developing animals flout prominent assumptions of ecological physiology. Comp. Biochem. Physiol. Part A Mol. Integr. Physiol. 141: 430–439.

Callier V., Nijhout F., 2011 Control of body size by oxygen supply reveals size-dependent and size-independent mechanisms of molting and metamorphosis. Proc. Natl. Acad. Sci. 108: 14664–14669.

Callier V., Nijhout F., 2012 Supply-side constraints are insufficient to explain the ontogenetic scaling of metabolic rate in the tobacco hornworm, *Manduca sexta* (F Seebacher, Ed.). PLoS One 7: e45455.

Callier V., Hand S., Campbell J., Biddulph T., Harrison J., 2015 Developmental changes in hypoxic exposure and responses to anoxia in *Drosophila melanogaster*. J. Exp. Biol. 218: 2927 -2934.

Carvalho M., Sampaio J., Palm W., Brankatschk M., Eaton S., *et al*., 2012 Effects of diet and development on the *Drosophila* lipidome. Mol. Syst. Biol. 8: 600.

Chance B., Williams G., 1955 Respiratory enzymes in oxidative phosphorylation: I. kinetics of oxygen utilization. J. Biol. Chem. 217: 383–394.

Charlesworth B., Charlesworth D., 2016 Population genetics from 1966 to 2016. Heredity 118: 2.

Church R., Robertson F., 1966 A biochemical study of the growth of *Drosophila melanogaster*. J. Exp. Zool. 162: 337–351.

Clark A., Wang L., Hulleberg T., 1995a P-element-induced variation in metabolic regulation in *Drosophila*. Genetics 139: 337 -348.

Clark A., Wang L., Hulleberg T., 1995b Spontaneous mutation rate of modifiers of metabolism in *Drosophila*. Genetics 139: 767 -779.

Clark A., Wang L., 1997 Epistasis in measured genotypes: *Drosophila* p-element insertions.

Genetics 147: 157–163.
Crawford D., Oleksiak M., 2007 The biological importance of measuring individual variation. J. Exp. Biol. 210: 1613 -1621.
Dlasková A., Špaček T., Škobisová E., Šantorová J., Ježek P., 2006 Certain aspects of uncoupling due to mitochondrial uncoupling proteins in vitro and in vivo. Biochim. Biophys. Acta - Bioenerg. 1757: 467–473.
Estabrook R., 1967 Mitochondrial respiratory control and the polarographic measurement of ADP : O ratios. Methods Enzymol. 10: 41–47.
Flowers J., Sezgin E., Kumagai S., Duvernell D., Matzkin L., *et al*., 2007 Adaptive evolution of metabolic pathways in *Drosophila*. Mol. Biol. Evol. 24: 1347–1354.
Frazier A., Thorburn D., Compton A., 2017 Mitochondrial energy generation disorders: genes, mechanisms and clues to pathology. J. Biol. Chem.
Gillespie J., 1999 The role of population size in molecular evolution. Theor. Popul. Biol. 55: 145–156.
Giorgio M., Trinei M., Migliaccio E., Pelicci P., 2007 Hydrogen peroxide: a metabolic by-product or a common mediator of ageing signals? Nat. Rev. Mol. Cell Biol. 8: 722.
Glazier D., 2005 Beyond the '3/4-power law': variation in the intra-and interspecific scaling of metabolic rate in animals. Biol. Rev. 80: 611–662.
Glazier D., 2014 Metabolic scaling in complex living systems. Systems 2: 451–540.
Glazier D., 2015 Is metabolic rate a universal 'pacemaker' for biological processes? Biol. Rev. 90: 377–407.
Graveley B., Brooks A., Carlson J., Duff M., Landolin J., *et al*., 2011 The deveopmental transcriptome of *Drosophila melanogaster*. Nature 471: 473–479.
Greenlee K., Montooth K., Helm B., 2014 Predicting performance and plasticity in the development of respiratory structures and metabolic systems. Integr. Comp. Biol. 54: 307–322.
Harris H., 1966 Genetics of man enzyme polymorphisms in man. Proc. R. Soc. London. Ser. B. Biol. Sci. 164: 298 -310.
Hoekstra L., Siddiq M., Montooth K., 2013 Pleiotropic effects of a mitochondrial–nuclear incompatibility depend upon the accelerating effect of temperature in *Drosophila*. Genetics 195: 1129 -1139.
Hoekstra L., Julick C., Katelyn M., Montooth K., 2018 Energy demand and the context-dependent effects of genetic interactions underlying metabolism. Evol. Lett. 2: 102–113.
Holmbeck M., Donner J., Villa-Cuesta E., Rand D., 2015 A *Drosophila* model for mito-nuclear diseases generated by an incompatible interaction between tRNA and tRNA synthetase. Dis. Model. Mech. 8: 843 -854.
Hubby J., Lewontin R., 1966 A molecular approach to the study of genic heterozygosity in natural populations. I. the number of alleles at different loci in *Drosophila pseudoobscura*. Genetics 54: 577–594.
Isler K., VanSchaik C., 2006 Metabolic costs of brain size evolution. Biol. Lett. 2: 557 -560.
Jeong H., Tombor B., Albert R., Oltvai Z., Barabási A., 2000 The large-scale organization of metabolic networks. Nature 407: 651.
Kimura M., 1983 *The Neutral Theory of Molecular Evolution*. Cambridge University Press, Cambridge.
Kurbalija N., Immonen E., Jelić M., AnĐelković M., Stamenković-Radak M., *et al*., 2014 Within-population genetic effects of mtDNA on metabolic rate in *Drosophila subobscura*.

J. Evol. Biol. 28: 338–346.

Laurie-Ahlberg C., Maroni G., Bewley G., Lucchesi J., Weir B., 1980 Quantitative genetic variation of enzyme activities in natural populations of *Drosophila melanogaster*. Proc. Natl. Acad. Sci. U. S. A. 77: 1073—1077.

Laurie-Ahlberg C., Wilton A., Curtsinger J., Emigh T., 1982 Naturally occuring enzyme activity variation in *Drosophila melanogaster*. I. sources of variation for 23 enzymes. Genetics 102: 191 -206.

Lewontin R., Hubby J., 1966 A molecular approach to the study of genic heterozygosity in natural populations. II. amount of variation and degree of heterozygosity in natural populations of *Drosophila pseudoobscura*. Genetics 54: 595–609.

Li H., Chawla G., Hurlburt A., Sterrett M., Zaslaver O., *et al*., 2017 *Drosophila* larvae synthesize the putative oncometabolite L-2-hydroxyglutarate during normal developmental growth. Proc. Natl. Acad. Sci. 114: 1353 -1358.

Lincet H., Icard P., 2014 How do glycolytic enzymes favour cancer cell proliferation by nonmetabolic functions? Oncogene 34: 3751.

Lunt S., Vander-Heiden M., 2011 Aerobic glycolysis: meeting the metabolic requirements of cell proliferation. Annu. Rev. Cell Dev. Biol. 27: 441–464.

Marden J., 2013 Nature's inordinate fondness for metabolic enzymes: why metabolic enzyme loci are so frequently targets of selection. Mol. Ecol. 22: 5743–5764.

Martin A., 1995 Metabolic rate and directional nucleotide substitution in animal mitochondrial DNA. Mol. Biol. Evol. 12: 1124–1131.

Meiklejohn C., Hartl D., 2002 A single mode of canalization. Trends Ecol. Evol. 17: 468–473.

Meiklejohn C., Holmbeck M., Siddiq M., Abt D., Rand D., *et al*., 2013 An incompatibility between a mitochondrial tRNA and Its nuclear-encoded tRNA synthetase compromises development and fitness in *Drosophila*. PLoS Genet. 9: e1003238.

Miettinen T., Björklund M., 2017 Mitochondrial function and cell size: an allometric relationship. Trends Cell Biol. 27: 393–402.

Mitchell-Olds T., Pedersen D., 1998 The molecular basis of quantitative genetic variation in central and secondary metabolism in *Arabidopsis*. Genetics 149: 739 -747.

Montooth K., Marden J., Clark A., 2003 Mapping determinants of variation in energy metabolism, respiration and flight in *Drosophila*. Genetics 165: 623 LP-635.

Montooth K., Meiklejohn C., Abt D., Rand D., 2010 Mitochondrial-nuclear epistasis affects fitness within species but does not contribute to fixed incompatibilities between species of *Drosophila*. Evolution 64: 3364–3379.

Nespolo R., Castañeda L., Roff D., 2007 Quantitative genetic variation of metabolism in the nymphs of the sand cricket, *Gryllus firmus*, inferred from an analysis of inbred-lines. Biol. Res. 40: 5–12.

O'Farrell P., 2004 How metazoans reach their full size: the natural history of bigness. In: Hall M, Raff M, Thomas G (Eds.), *Cell Growth: Control of Cell Size*, Cold Spring Harbor Laboratory Press, New York, pp. 1–22.

Pekny J., Smith P., Marden J., 2018 Enzyme polymorphism, oxygen and injury: a lipidomic analysis of flight-induced oxidative damage in a succinate dehydrogenase d (Sdhd)-polymorphic insect. J. Exp. Biol. 221.

Porter R., Brand M., 1993 Body mass dependence of H^+ leak in mitochondria and its relevance to metabolic rate. Nature 362: 628.

Porter R., Hulbert A., Brand M., 1996 Allometry of mitochondrial proton leak: influence of

membrane surface area and fatty acid composition. Am. J. Physiol. Integr. Comp. Physiol. 271: R1550–R1560.

Ravasz E., Somera A., Mongru D., Oltvai Z., Barabási A., 2002 Hierarchical organization of modularity in metabolic networks. Science. 297: 1551–1555.

Ricklefs R., 2003 Is rate of ontogenetic growth constrained by resource supply or tissue growth potential? A comment on West *et al*.'s model. Funct. Ecol. 17: 384–393.

Sears K., Kerkhoff A., Messerman A., Itagaki H., 2012 Ontogenetic scaling of metabolism, growth, and assimilation: testing metabolic scaling theory with *Manduca sexta* larvae. Physiol. Biochem. Zool. 85: 159–173.

Shin O., Yasuo I., 1984 Allometric relationship between tissue respiration and body mass in the carp. Comp. Biochem. Physiol. A. Mol. Integr. Physiol. 77: 415–418.

Shin O., Yasuo I., 1993 Allometric relationship between tissue respiration and body mass in a marine teleost, porgy *Pagrus major*. JournalComparative Biochem. Physiol. Part A Physiol. 105: 129–133.

Somero G., Lockwood B., Tomanek L., 2017 *Biochemical adaptation:response to environmental challenges from life's origins to the anthropocene*.

Strogatz S. H., 2001 Exploring complex networks. Nature 410: 268.

Szczepanowska J., Malinska D., Wieckowski M., Duszynski J., 2012 Effect of mtDNA point mutations on cellular bioenergetics. Biochim. Biophys. Acta - Bioenerg. 1817: 1740–1746.

Tennessen J., Baker K., Lam G., Evans J., Thummel C., 2011 The *Drosophila* estrogen-related receptor directs a metabolic switch that supports developmental growth. Cell Metab. 13: 139–148.

Tennessen J. M., Thummel C. S., 2011 Coordinating growth and review maturation — insights from *Drosophila*. Curr. Biol. 21: R750–R757.

Tennessen J. M., Bertagnolli N. M., Evans J., Sieber M. H., Cox J., *et al*., 2014 Coordinated metabolic transitions during Drosophila embryogenesis and the onset of aerobic glycolysis. G3 Genes|Genomes|Genetics 4: 839–850.

Tieleman I., Versteegh M., Fries A., Helm B., Dingemanse N., *et al*., 2009 Genetic modulation of energy metabolism in birds through mitochondrial function. Proc. R. Soc. B Biol. Sci. 276: 1685 LP-1693.

Tishkoff S., Varkonyi R., Cahinhinan N., Abbes S., Argyropoulos G., *et al*., 2001 Haplotype diversity and linkage disequilibrium at human G6PD: recent origin of alleles that confer malarial resistance. Science. 293: 455 LP-462.

Tomanek L., Zuzow M., 2010 The proteomic response of the mussel congeners *Mytilus galloprovincialis* and *M. trossulus* to acute heat stress: implications for thermal tolerance limits and metabolic costs of thermal stress. J. Exp. Biol. 213: 3559 -3574.

VanDyken D., Wade M., 2010 The genetic signature of conditional expression. Genetics 184: 557 -570.

Verrelli B., Eanes W., 2001 The functional impact of Pgm amino acid polymorphism on glycogen content in *Drosophila melanogaster*. Genetics 159: 201–210.

Villa-Cuesta E., Holmbeck M., Rand D., 2014 Rapamycin increases mitochondrial efficiency by mtDNA-dependent reprogramming of mitochondrial metabolism in *Drosophila*. J. Cell Sci. 127: 2282 -2290.

Vollmer J., Casares F., Iber D., 2017 Growth and size control during development. Open Biol. 7.

VonBertalanffy L., Pirozynski W., 1953 Tissue respiration, growth, and basal metabolism. Biol. Bull. 105: 240–256.

872 Waddington C., 1942 Canalization of development and the inheritence of acquired characters.
873 Nature 150: 563.
874 Waddington C., 1957 *The strategy of the genes: a discussion of some aspects of theoritical*
875 *biology*. London: George Allen & Unwin, Ltd.
876 Ward P. S., Thompson C. B., 2012 Signaling in control of cell growth and metabolism. Cold
877 Spring Harb. Perspect. Biol. 4.
878 Warton D., Wright I., Falster D., Westoby M., 2006 Bivariate line-fitting methods for allometry.
879 Biol. Rev. 81: 259–291.
880 Watt W., 1977 Adaptation at specific loci. I. natural selection on phosphogluco isomerase of
881 *Colias* butterflies: biochemical and population aspects. Genetics 87: 177 -194.
882 Watt W., Cassin R., Swan M., 1983 Adaptation at specific loci. III. field behavior and
883 srvivorship differences among *Colias* PGI genotypes are predictable from in vitro
884 biochemistry. Genetics 103: 725 -739.
885 Watt W., Wheat C., Meyer E., Martin J., 2003 Adaptation at specific loci. VII. natural selection,
886 dispersal and the diversity of molecular–functional variation patterns among butterfly
887 species complexes (*Colias*: Lepidoptera, Pieridae). Mol. Ecol. 12: 1265–1275.
888 Zhang C., Montooth K., Calvi B., 2017 Incompatibility between mitochondrial and nuclear
889 genomes during oogenesis results in ovarian failure and embryonic lethality. Development
890 144: 2490–2503.
891